XBeach testbed report

status update trunk_default

Revision: 2158 (trunk)

August 1, 2011

XBeach testbed report

Published and printed by:

Deltares
Rotterdamseweg 185
p.o. box 177
2600 MH Delft
The Netherlands

telephone: +31 88 335 85 85
fax: +31 88 335 85 82
e-mail: info@deltares.nl
www: http://www.deltares.nl

For support contact:

telephone: +31 88 335 85 55
fax: +31 88 335 81 11
e-mail: xbeach@deltares.nl
www: http://www.xbeach.org/

Contents

Chapter 1

Introduction

1.1 Introduction to the XBeach model

The devastating effects of hurricanes on low-lying sandy coasts, especially during the 2004 and 2005 seasons have pointed at an urgent need to be able to assess the vulnerability of coastal areas and (re-)design coastal protection for future events, and also to evaluate the performance of existing coastal protection projects compared to 'do-nothing' scenarios. In view of this the Morphos-3D project was initiated by USACE-ERDC, bringing together models, modelers and data on hurricane winds, storm surges, wave generation and nearshore processes. As part of this initiative an open-source program, XBeach for eXtreme Beach behaviour, has been developed to model the nearshore response to hurricane impacts. The model includes wave breaking, surf and swash zone processes, dune erosion, overwashing and breaching.

Existing tools to assess dune erosion under extreme storm conditions assume alongshore uniform conditions and have been applied successfully along relatively undisturbed coasts (Vellinga, 1986, Steetzel, 1993, Nishi and Kraus, 1996, Larson et al., 2004), but are inadequate to assess the more complex situation where the coast has significant alongshore variability. This variability may result from anthropogenic causes, such as the presence of artificial inlets, sea walls, and revetments, but also from natural causes, such as the variation in dune height along the coast or the presence of rip channels and shoals on the shoreface (Thornton et al., 2007). A particularly complex situation is found when barrier islands protect storm impact on the main land coast. In that case the elevation, width and length of the barrier island, as well as the hydrodynamic conditions (surge level) of the back bay should be taken into account to assess the coastal response. Therefore, the assessment of storm impact in these more complex situations requires a two-dimensional process-based prediction tool, which contains the essential physics of dune erosion and overwash, avalanching, swash motions, infragravity waves and wave groups.

With regard to dune erosion, the development of a scarp andepisodic slumping after undercutting is a dominant process (van Gent et al., 2008). This supplies sand to the swash and surf zone that is transported seaward by the backwash motion and by the undertow; without it the upper beach scours down and the dune erosion process slows down considerably. One-dimensional (cross-shore) models such as DUROSTA (Steetzel, 1993) focus on the underwater offshore transport and obtain the supply of sand by extrapolating these transports to the dry dune. Overton and Fisher (1988), Nishi and Kraus (1996) focus on the supply of sand by the dune based on the concept of wave impact. Both approaches rely on heuristic estimates of

the runup and are well suited for 1D application but difficult to apply in a horizontally 2D setting. Hence, a more comprehensive modelling of the swash motions is called for.

Swash motions are up to a large degree a result from wave-group forcing of infragravity waves (Tucker, 1954). Depending on the beach configuration and directional properties of the incident wave spectrum both leaky and trapped infragravity waves contribute to the swash spectrum (Huntley et al., 1981). Raubenheimer and Guza (1996) show that incident band swash is saturated, infragravity swash is not, therefore infragravity swash is dominant in storm conditions. Models range from empirical formulations (e.g. Stockdon et al., 2006) through analytical approaches (Schaeffer, 1994, Erikson et al., 2005) to numerical models in 1D (e.g. List, 1992, Roelvink, 1993b) and 2DH (e.g. van Dongeren et al., 2003, Reniers et al., 2004a, 2006). 2DH wavegroup resolving models are well capable of describing low-frequency motions. However, for such a model to be applied for swash, a robust drying/flooding formulation is required.

1.2 Model approach and innovations

Our aim is to model processes in different regimes as described by Sallenger (2000). He defines an Impact Level to denote different regimes of impact on barrier islands by hurricanes, which are the 1) swash regime, 2) collision regime, 3) overwash regime and 4) inundation regime. The approach we follow to model the processes in these regimes is described below.

To resolve the swash dynamics the model employs a novel 2DH description of the wave groups and accompanying infragravity waves over an arbitrary bathymetry (thus including bound, free and refractively trapped infragravity waves). The wave-group forcing is derived from the time-varying wave-action balance e.g. Phillips (1977) with a dissipation model for use in combination with wave groups (Roelvink, 1993a). A roller model (Svendsen, 1984; Nairn et al., 1990; Stive and de Vriend, 1994) is used to represent momentum stored in surface rollers which leads to a shoreward shift in wave forcing.

The wave-group forcing drives infragravity motions and both longshore and cross-shore currents. Wave-current interaction within the wave boundary layer results in an increased wave-averaged bed shear stress acting on the infragravity waves and currents (e.g. Soulsby et al., 1993 and references therein). To account for the randomness of the incident waves the description by Feddersen et al. (2000) is applied which showed good skill for longshore current predictions using a constant drag coefficient (Ruessink et al., 2001).

During the swash and collision regime the mass flux carried by the waves and rollers returns offshore as a return flow or a rip-current. These offshore directed flows keep the erosion process going by removing sand from the slumping dune face. Various models have been proposed for the vertical profile of these currents (see Reniers et al., 2004b for a review). However, the vertical variation is not very strong during extreme conditions and has been neglected for the moment.

Surf and swash zone sediment transport processes are very complex, with sediment stirring by a combination of short-wave and long-wave orbital motion, currents and breaker-induced turbulence. However, intra-wave sediment transports due to wave asymmetry and wave skewness are expected to be relatively minor compared to long-wave and mean current contributions (van Thiel de Vries et al., 2008). This allows for a relatively simple and transparent formulation according to Soulsby & Van Rijn (Soulsby, 1997) in a shortwave averaged but wave-group resolving model of surf zone processes. This formulation has been applied successfully in describing the generation of rip channels (Damgaard et al., 2002 Reniers et al.,

2004a) and barrier breaching (Roelvink et al., 2003).

In the collision regime, the transport of sediment from the dry dune face to the wet swash, i.e. slumping or avalanching, is modeled with an avalanching model accounting for the fact that saturated sand moves more easily than dry sand, by introducing both a critical wet slope and dry slope. As a result slumping is predominantly triggered by a combination of infragravity swash runup on the previously dry dune face and the (smaller) critical wet slope.

During the overwash regime the flow is dominated by lowfrequency motions on the time scale of wave groups, carrying water over the dunes. This onshore flux of water is an important landward transport process where dune sand is being deposited on the island and within the shallow inshore bay as overwash fans (e.g. Leatherman et al., 1977; Wang and Horwitz, 2007). To account for this landward transport some heuristic approaches exist in 1D, e.g. in the SBeach overwash module (Larson et al., 2004) which cannot be readily applied in 2D. Here, the overwash morphodynamics are taken into account with the wave-group forcing of low-frequency motions in combination with a robust momentum-conserving drying/flooding formulation (Stelling and Duinmeijer, 2003) and concurrent sediment transport and bed-elevation changes.

Breaching of barrier islands occurs during the inundation regime, where a new channel is formed cutting through the island. Visser (1998) presents a semi-empirical approach for breach evolution based on a schematic uniform cross-section. Here a generic description is used where the evolution of the channel is calculated from the sediment transports induced by the dynamic channel flow in combination with avalanche-triggered bank erosion.

1.3 XBeach testbed

The XBeach code and related functionalities develop fast. As a result there is a need from modelers and code developers to develop a tool that gives insight in the effect of code developments on model performnace. The XBeach testbed tries to fulfill this need by running a range of tests including analytical solutions, laboratory tests and practical field cases every week with the latest code.

Chapter 2

Release information

2.1 Release notes

We have been working on a lot of cool stuff that still needs to be described in more detail:

- hard structures
- multiple sediment fractions
- bed load and suspended load
- output options
- wave schemes
- non-hydrostatic model
- wave shap parameterization
- drifters
- river outflow
- boundary condition stuff
- ...

2.2 Change log

2.2.1 trunk

Chapter 3

Overview

In the table below the statuses of all tests found in the testbed are summarized. In case a test is ignored or has failed, the corresponding message is given in the column “Message”. Please note that success or failure of the test runs are given in column “Run status”, while the success or failure of the Matlab analyses are given in column “Matlab status”. The last columns provide an overview of the main characteristics of each test.

Tests can be run multiple times using different settings. Different runs are identified by a run name, which follows after the test name and a dot sign. If a test is run once only, it is common use to name the run *default*.

Table 3.1: Status overview testbed tests

Binary	Test	Run	Status	Matlab	Default run	Configuration	Waves*	Water levels**	Fractions	Morphology	Hard layers	Groundwater flow

* ST = stationary, WG = wave groups, NH = non-hydrostatic
** C = constant, V = varying

Chapter 4

Hydrodynamic tests

4.1 Long wave propagation

The purpose of the this test is to check if the NSWE numerical scheme is not too dissipative and that it does not create large errors in propagation speed.

A long wave with a small amplitude of $0.01m$ and period of $80s$ was sent into a domain of $5m$ depth, grid size of $5m$ and a length of $1km$. At the end, a fully reflecting wall is imposed. The wave length in this case should be $\sqrt{9.81 \cdot 5} \cdot 80 = 560m$. The velocity amplitude should be $\sqrt{g/h} \cdot A = \sqrt{9.81/5} \cdot 0.01 = 0.014m$. After the wave has reached the wall, a standing wave with double amplitude should be created.

Figure 4.1

Figure 4.2

As Figure 4.1 and Figure 4.2 should show, the model accurately represents this situation. There is hardly any dissipation, the wave length is very close to what it should be and there is no reflection off the seaward boundary.

4.2 Carrier and Greenspan

The purpose of this test is to check the ability of the model to represent runup and rundown of non-breaking long waves. To this end, a comparison was made with the analytical solution of the NSWE by Carrier and Greenspan (1958), which describes the motion of harmonic, non-breaking long waves on a plane sloping beach without friction.

A free long wave with a wave period of 32 seconds and wave amplitude of half the wave breaking amplitude ($a_{in} = 0.5 \cdot a_{br}$) propagates over a beach with constant slope equal to $1/25$. The wave breaking amplitude is computed as $a_{br} = {}^{1}/_{\sqrt{128}\cdot\pi^3} \cdot s^{2.5} \cdot T^{2.5} \cdot g^{1.25} \cdot h_0^{-0.25} = 0.0307 meter$, where s is the beach slope, T is the wave period and h_0 is the still water depth at the seaward boundary. The grid is non uniform and consists of 160 grid points. The grid size dx is decreasing in shoreward direction and is proportional to the (free) long wave celerity ($\sqrt{g \cdot h}$).The minimum grid size in shallow water was set at $dx = 0.1 meter$.

To compare XBeach output to the analytical solution of Carrier and Greenspan, the first are non-dimensionalized with the beach slope s, the acceleration of gravity g, the wave period T, a horizontal length scale L_x and the vertical excursion of the swash motion A. The horizontal length scale L_x is related to the wave period via $T = \sqrt{L_x/g \cdot s}$ and the vertical excursion of the swash motion A is expressed as: $A = a_{in} \cdot {}^{\pi}/_{\sqrt{0.125 \cdot s \cdot T \cdot \sqrt{g/h_0}}}$

Figure 4.3

The two panels in Figure 4.3 compare the XBeach results with the analytical solution. The agreement should be reasonably well, though there are small deviations in the water level near the water line and the flow velocities seem to lag slightly on the analytical solution during the second part of the run down. Since the analytical solution is stationary, numerical output over multiple waves is shown in Figure 4.3, verifying that also the numerical solution is reasonably stationary.

Carrier, G.F., and Greenspan, H.P., *Water waves of finite amplitude on a sloping beach.* Journal of Fluid Mechanics, 1958, vol. 4, 97 - 109

4.3 Boers 1C

Boers (1996) performed experiments with irregular waves in the physical wave flume at Delft University of Technology with a length of 40 meters and a width of 0.8 m. The flume is equipped with a hydraulically driven, piston type wave generator with second-order wave generation and Active Reflection Compensation. Boers ran waves over a concrete bar-trough beach, which was modelled after the Delta Flume experiments. He ran three different irregular wave conditions, but in this report we will focus on case 1C, a Jonswap spectrum with $H_{m,0} =$ 0.1m and $T_p = 3.3$s. The surface elevation was measured in 70 locations shown in Figure 4.4.

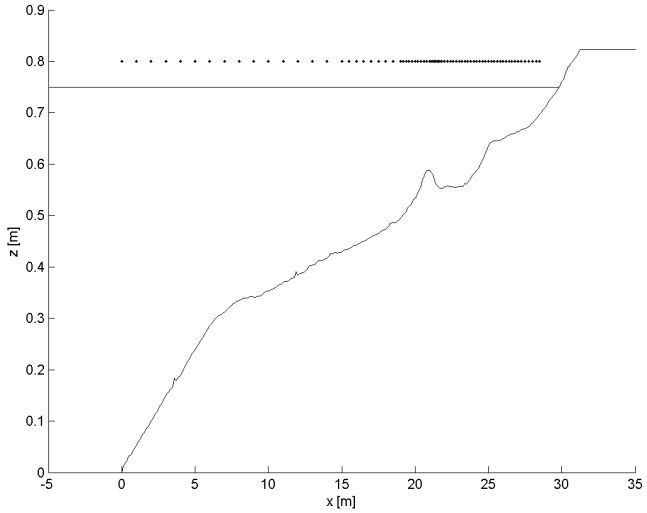

Figure 4.4

The comparison between the model and the data for the wave height transformation of the short waves and the long waves (defined as waves with a frequency greater than $f_p/2$ and less than $f_p/2$, respectively) is shown in Figure 4.5.

The top dark blue line indicates the short wave height transformation, which should compare well with the measurements, except for details around the breakpoint. The green line and stars indicate the mean (steady) set-up which should be well-predicted, except in the trough region (x=21-25 m). The red lines and stars indicate the total (incoming and reflected) low frequency wave, which is slightly overpredicted in the shoaling zone (up to the breakpoint) and stays too large after that.

The observational data is separated into incoming and reflected long wave components using an array of wave gauges (Bakkenes, 2002) and the numerical data has been separated into two components using co-located surface elevation and velocity information. The incoming long wave (cyan line) follows the observations (cyan stars) with a notable overprediction seaward of the breaking zone. The reflected long waves (black lines) match the observations (black stars) quite well.

Figure 4.5

The model should perform reasonably well against the data for this well-measured but complex case.

Bakkenes, H.J., 2002. *Observation and seperation of bound and free low-frequency waves in the nearshore zone.* MSc Thesis, Delft University of Technology, Delft, The Netherlands.

Boers, M. (1996), *Simulation of a Surf Zone with a Barred Beach, Part 1: Wave heights and Wave breaking*, Communications on Hydraulic and Geotechnical Eng., Delft University of Technology, Civil Engineering, Report No. 96-5, 116 p.

4.4 Zelt

The verification cases so far considered solely the cross-shore dimension and assumed a longshore uniform coast. In the following cases the potential of the model to predict coastal and dune erosion in situations that include the two horizontal dimensions is further examined. A first step towards a 2DH response is to verify that the 2DH forcing by surge run-up and rundown is accurately modelled by testing not against Zelt (1986), but actually Özkan-Haller & Kirby (1997). The reason is that Zelt modeled the NSW equations including some dispersive and dissipative terms, which the present model does not have. For that reason, we also compared our model to the results of Özkan-Haller & Kirby (1997) who modeled the NSW equations using a Fourier-Chebyshev Collocation method, which does not have any numerical dissipation or dispersion errors. They use a moving, adapting grid with a fixed Δy (which is equal to the present model's Δy in this comparison) but with a spatially and temporally varying Δx so that the grid spacing in x near the shoreline is very small. In the present model Δx is set equal to Δy, which means that we can expect to have less resolution at the shoreline than Özkan-Haller & Kirby (1997).

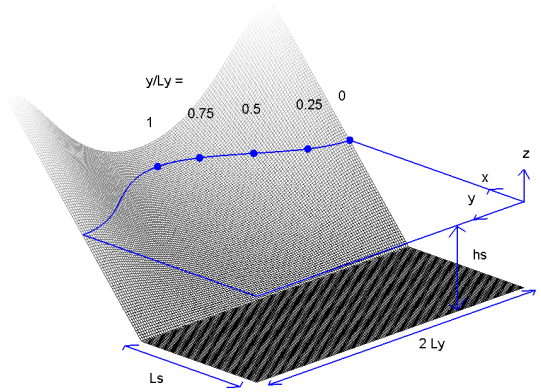

Figure 4.6

Figure 4.6 shows the definition sketch of the concave beach bathymetry in the present coordinate system, converted from the original system by Zelt (1986). The bathymetry consists of a flat bottom part and a beach part with a sinusoidally varying slope. For Zelt (1986)'s fixed parameter choice of $\sqrt{\beta} = \frac{h_s}{L_y} = \frac{4}{10\pi}$, the bathymetry is given by

$$\mathrm{h} = \{$$

$$\begin{array}{ll} h_s & , \quad x \leq L_s \\ h_s - \frac{0.4(x-L_s)}{3-\cos\left(\frac{\pi y}{L_y}\right)} & , \quad x > L_s \end{array}$$

where h_s is the shelf depth, L_s is the length of the shelf in the modeled domain and L_y is the length scale of the longshore variation of the beach. This results in a beach slope of $h_x = \frac{1}{10}$ in the center of the bay and of $h_x = \frac{1}{5}$ normal to the "headlands". In the following we chose $L_y = 8\,m$, which determines $h_s = 1.0182\,m$. We set $L_s = L_y$. Different values for L_s only cause phase shifts in the results, but no qualitative difference, so this parameter is not important in this problem. Also indicated in the figure are the five stations where the vertical run-up (the surface elevation at the shoreline) will be measured.

At the offshore ($x = 0$) boundary we specify an incoming solitary wave, which in dimensional form reads

$$\zeta_i(t) = \alpha h_s \mathrm{sech}^2\left(\sqrt{\tfrac{3g}{4h_s}\alpha(1+\alpha)}(t-t_o)\right)$$

which is similar to Zelt (1986)'s Eq. (5.3.7). The phase shift t_o is chosen such that the surface elevation of the solitary wave at $t = 0$ is 1% of the maximum amplitude. The only parameter yet to be chosen is α. We will compare our model to Zelt's case of $\alpha = \frac{H}{h_s} = 0.02$, where H is the offshore wave height. Zelt found that the wave broke for a value of $\alpha = 0.03$, so the present test should involve no breaking, but has a large enough nonlinearity to exhibit a pronounced two-dimensional run-up.

Any outgoing waves will be absorbed at the offshore boundary by the absorbing-generating boundary condition. At the lateral boundaries $y = 0$ and $y = 2\,L_y$ we specify a no-flux (wall) boundary condition following Zelt. The model equations used in this test are the nonlinear shallow water equations without forcing or friction. The numerical parameters are $\Delta x = \Delta y = \frac{1}{8}\,m$ with a Courant number $\nu = 0.7$.

Figure 4.7

The first panel in Figure 4.7 shows the vertical runup normalized with the offshore wave height H as a function of time, which is normalized by $\sqrt{g\,h_s}/L_y$ at the 5 cross-sections indicated in Figure 4.6. The solid lines represent the present model results, while the dashed lines denotes Ozkan & Kirby (1997)'s numerical results. We should see that the agreement is generally good, except that the present model does not capture the second peak in the time series at $y/Ly = 1$ very well. This secondary peak or "ringing" is due to the wave energy that is trapped along the coast and propagates towards the midpoint of the bay (Zelt, 1986). It is suspected that this focusing mechanism is not properly captured, because the present method approximates the shoreline as a staircase pattern, which in effect lengthens the shoreline. Also, the spatial derivatives are not evaluated parallel and perpendicular to the actual shoreline but in the fixed x and y directions. The agreement at the locations $y/Ly = 0.25$, $y/Ly = 0.5$ and $y/Ly = 0.75$ is generally good despite the large gradient of the local shoreline relative to our grid.

The second panel in Figure 4.7 shows the maximum vertical run-up and run-down, normalized by H, versus the alongshore coordinate y. The maximum runup should agree well with Ozkan & Kirby (1997), but that the maximum rundown is not represented well in the center of the domain. The 'wiggles' in the solid line are evidence of the staircasing of the shoreline: since the shoreline is not treated as a continuous but rather as a discrete function, so is the runup in the individual nodes.

Table 4.1: Error statistics Zelt Case 1

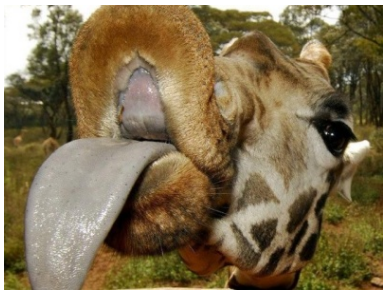

In conclusion, the shoreline boundary condition agrees well with the analytical solutions for the longshore uniform case but shows some discrepancies for the case of a concave beach, which can be attributed to the "staircase" discretization of the shoreline. The above results are consistent with the results obtained with the SHORECIRC model which is based on similar hydrodynamic equations, see Van Dongeren and Svendsen (1997), and show that also the current model is capable of representing run-up and run-down.

Özkan-Haller, H.T. and J.T. Kirby (1997). *A Fourier-Chebyshev collocation method for the shallow water equations including shoreline runup.* Applied Ocean Research, 19, pp. 21-34.

Zelt, J.A. (1986). *Tsunamis: the response of harbours with sloping boundaries to long wave excitation.* Doctoral dissertation, Rep. No. KH-R-47, W.M. Keck Laboratory of Hydraulics and Water Resources, Division of Engineering and Applied Science, California Institute of Technology, Pasadena, CA, 318 p.

4.5 Delilah

In order to verify the 2DH hydrodynamics of XBeach when forced by directionally-spread short waves, a simulation is set up to compare model results to field measurements. In this case the DELILAH field experiment at Duck, North Carolina is selected as a suitable test location. The period that is modeled is October 13th 1990, which was a stormy day, between 16:00 and 17:00 hours. The significant wave height at 8 m water depth was 1.81 m, with a peak period of 10.8 s and a mean angle of incidence of -16^o relative to the shoreward normal. This period is selected because the wave conditions are energetic enough to generate a significant infragravity wave component and the incident wave spectrum is sufficiently narrow-banded to justify the assumptions in the model boundary conditions. The model is forced with the wave spectrum measured at 8 m water depth (Birkemeier et al., 1997). A measured tidal signal is imposed on the model boundaries of which the mean level is 0.69 m above datum. The slope of the wave front in the roller model is set to 0.05, which is found to be a slight improvement over the value of 0.10 used in the previous sections. A constant grid size of 5 m in cross shore and 10 m in longshore direction is used. The resolution of the wave model in directional space is 15^o. The model is set to generate output at the location of the primary cross shore measurement array, gauge numbers 10, 20, 30, 40, 50, 60, 70, 80 and 90 (Figure 4.8).

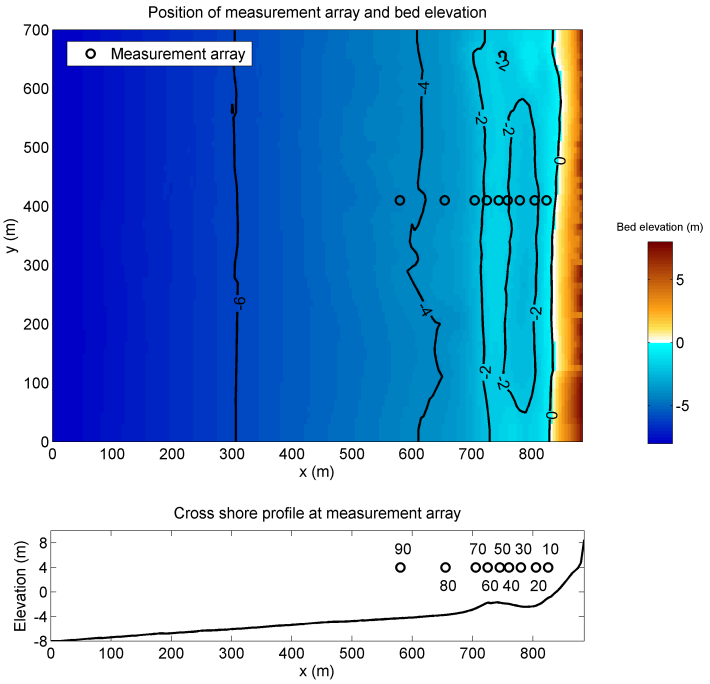

Figure 4.8

The modeled time-averaged wave heights of the short waves are compared to the time-averaged wave heights measured at the gauges. These results are shown in the first panel of Figure 4.9. Unfortunately, no data exist for gauge number 60.

The infragravity wave height is calculated as follows (van Dongeren et al., 2003):

$$H_{rms,low} = \sqrt{8 \int_{0.005Hz}^{0.05Hz} Sdf}$$

The second panel of Figure 4.9 should show that the XBeach model overestimates the infragravity wave height, but does follow the measured cross shore trend well.

The measured and modelled time-averaged longshore current are shown in the third panel of Figure 4.9. It can be seen that the model strongly under predicts the longshore current in the trench between measurement gauge 60 and the shore. Further calibration of the short wave and roller parameters is required in order to improve the simulated longshore current in this trough. The correlation coefficient, scatter index, relative bias and Brier Skill Score for the simulation are shown in Table 4.2.

Figure 4.9: DELILAH field experiment 1990. First panel: Time-averaged measured (squares) and modelled (line) RMS-wave height of the short waves. Second panel: Time-averaged measured (squares) and modeled (line) RMS-wave height of the infragravity waves. Third panel: Time-averaged measured (squares) and modeled (line) longshore velocity. Fourth panel: Cross shore profile at the location of the measurement gauge array with the positions of the gauges (crosses).

Table 4.2

The modeled and measured sea surface elevation spectra at all nine gauge locations are shown in Figure 4.10. Note that the modeled surface elevation spectra only contain low frequency components associated with wave groups. The figure shows a migration of energy from high to low frequencies in shoreward direction in the measured spectra. The simulated spectra reproduce well the trend of increasing energy in the low frequency band in shoreward direction, but the amount of energy in the simulated low frequency band is less than in the measurements. In conclusion it can be stated that the model reproduces to a high degree of accuracy the short wave transformation in the shoaling and breaker zone. The transfer of energy from high to low frequencies in the model has qualitative skill. The longshore velocity in the nearshore requires additional calibration of the short wave and roller parameters.

Figure 4.10: DELILAH field experiment 1990: Measured (solid line) and modelled (dashed line) surface elevation spectra for nine locations in the primary cross shore array. Gauge 90 is the most seaward.

Birkemeier, W.A., C. Donoghue, C. E. Long, K. K. Hathaway, and C. F. Baron (1997) *1990 DELILAH Nearshore Experiment: Summary report*, Tech. Rep. CHL-97-4-24, Field Res. Facil., U.S. Army Corps of Eng., Waterways Exper. Stn., Vicksburg., Miss.

Van Dongeren, A., A. Reniers, J. Battjes, and I. Svendsen (2003), *Numerical modeling of infragravity wave response during DELILAH*, J. Geophys. Res., 108(C9), 3288, doi:10.1029/2002JC001332.

Chapter 5

Morphological laboratory tests

5.1 Scale relations

5.1.1 M1263-I

Figure 5.1: Overview of Brier Skill Scores

5.1.2 M1263-II

Figure 5.2: Overview of Brier Skill Scores

5.1.3 M1263-III

5.1.3.1 Test 1

The cross-shore profile is based on a simplified profile which is considered as more or less representative for most of the Dutch coast. This profile is often referred to as *reference profile*. It has been scaled according to:

$n_d = 5$

$n_l = n_d(n_d/n_w^2)^{0.28} = 5(5/1)^{0.28} = 5^{1.28} = 7.85$

Sand from prototype with $D_{50} = 225$ μm was used as a bed material.

This experiment was carried out with constant hydraulic conditions:

wave height	1.5 m
wave period	5.4 s

Figure 5.3 shows the profile development in time, simulated compared to measured. Table 5.1 shows the Brier Skill Scores at the moments in time which are comparable to profile measurements.

Figure 5.3

Figure 5.4

Table 5.1

5.1.3.2 Test 2

In this experiment, the same cross-shore profile as in Test 1.

Sand from prototype with $D_{50} = 225$ μm was used as a bed material.

This experiment was carried out with constant hydraulic conditions:

wave height	1.5 m
wave period	5.4 s

Figure 5.5 shows the profile development in time, simulated compared to measured. Table 5.2 shows the Brier Skill Scores at the moments in time which are comparable to profile measurements.

Figure 5.5

Figure 5.6

Table 5.2

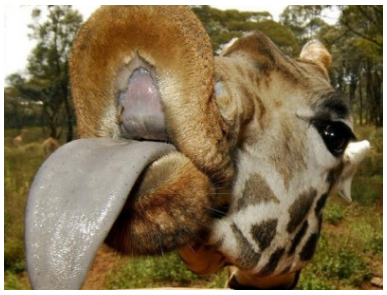

5.1.3.3 Test 3

In this experiment, the same cross-shore profile as in Test 1 and 2.

Sand from prototype with $D_{50} = 225$ μm was used as a bed material.

This experiment was carried out with time varying hydraulic conditions (Figure 5.7), of which the maximum values were:

wave height	1.5 m
wave period	5.4 s

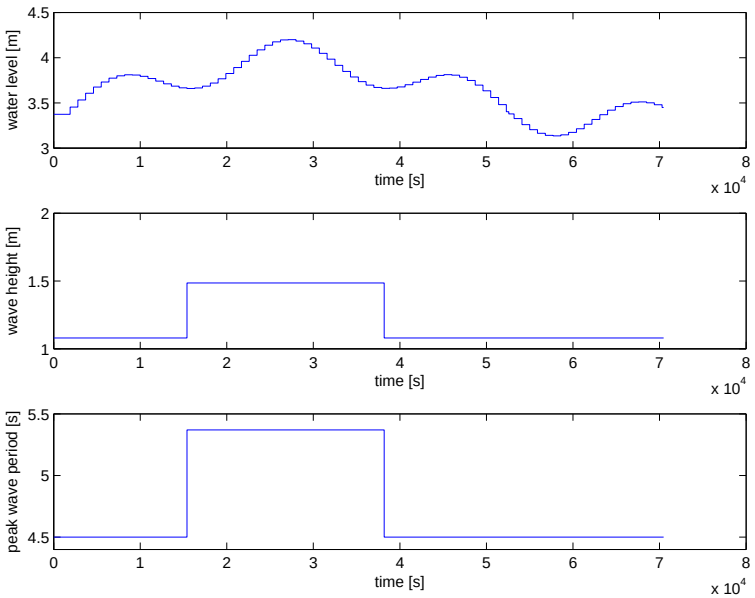

Figure 5.7

Figure 5.8 shows the profile development in time, simulated compared to measured. Table 5.3 shows the Brier Skill Scores at the moments in time which are comparable to profile measurements.

Figure 5.8

Figure 5.9

Table 5.3

5.1.3.4 Test 4

The cross-shore profile in this experiment is a representation of a profile at the Delfland coast. It has been scaled according to:

$n_d = n_H = n_L = {n_T}^2 = 3.27$

$n_l = (3.27)^{1.28} = 4.56$

$n_t = (n_d)^{0.5} = (3.27)^{0.5} = 1.81$

Sand from prototype with $D_{50} = 225$ μm was used as a bed material.

This experiment was carried out with time varying hydraulic conditions (Figure 5.10), of which the maximum values were:

wave height	1.85 m
wave period	5.0 s

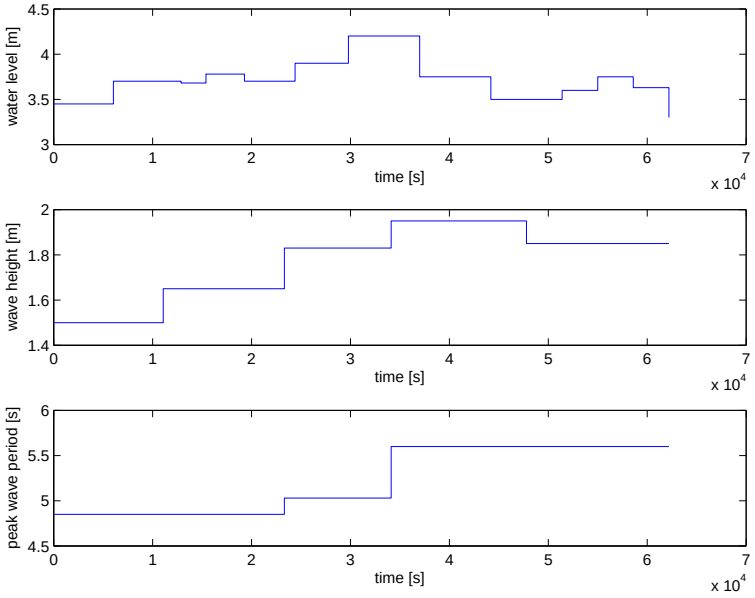

Figure 5.10

Figure 5.11 shows the profile development in time, simulated compared to measured. Table 5.4 shows the Brier Skill Scores at the moments in time which are comparable to profile measurements.

Figure 5.11

Figure 5.12

Table 5.4

5.1.3.5 Test 5

The cross-shore profile in this experiment was derived from the reference profile.

Figure 5.13 shows the profile development in time, simulated compared to measured. Table 5.5 shows the Brier Skill Scores at the moments in time which are comparable to profile measurements.

Figure 5.13

Figure 5.14

Table 5.5

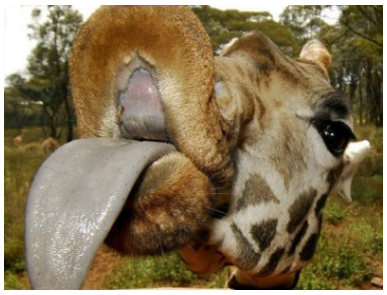

5.2 Large scale tests

5.2.1 Revetments

5.2.1.1 H298: Modelonderzoek duinvoetverdedigingen

5.2.1.2 T1

In test T1 of the Deltflume H298 series (Steetzel,1987) scour hole development in front of a dune revetment is ivestigated. The test was carried out at a depth scale nd = 5 (Vellinga, 1986) and the initial profile in the flume correponds to the reference profile for the Dutch Holland coast. At the dune foot (located at x = 193 m from the wave board and z = 3.80 m above the flumes floor) a concrete revetment is applied that covers almost the whole dune face (slope of 1:1.8). The lower end of the revetment is located at z = 2.5 m and the top end at z = 6.2 m. The test was conducted with a constant water level (set at z = 4.2 m) and wave conditions that correpsond to a Pierson Moskowitz spectrum with Hm0 = 1.52 m and Tp = 5.37s. The sand applied in the test has a median grain diameter (D_{50}) of approximately 210 um.

Simulated and measured profile development during T1 are compared in (Figure 5.15). In the physical experiment the scour hole devlops till a depth of z = 2.59 m above after seven hours simulation (is 1.21 meter below the dune foot). Computed bedlevel changes for sources and sinks (sourcesink=1) versus sediment transport gradients (sourcesink=0) are comparable. Without any relevant model improvements it is concluded that XBeach underestimates the erosion depth at the toe of the revetment. It seems an explaination may be found in simulated sediment suspensions in the proximity of the revtment, which are underestimated with a factor two (Figure 5.16). The simulated mean flow is supposed to be in reasonable agreement with measurements.

Figure 5.15

Figure 5.16

Table 5.6

Steetzel, H.J., 1987. Systematic reserach on the effectiveness of dune toe revetments, Large

scale model investigation (in Dutch), Report H298-I, Delft Hydraulics, Delft, The Netherlands.

5.2.1.3 T2

In test T2 ...

Simulated and measured profile development during T2 are compared in (Figure 5.17). ...

Figure 5.17

Figure 5.18

Steetzel, H.J., 1987. Systematic reserach on the effectiveness of dune toe revetments, Large scale model investigation (in Dutch), Report H298-I, Delft Hydraulics, Delft, The Netherlands.

5.2.1.4 H4731: Influence of collapsed revetments on dune erosion

5.2.2 LIP experiments

5.2.2.1 Dune erosion

This model test, described in Arcilla et al. (1994), concerns extreme conditions with a raised water level at 4.58 m above the flume bottom, a significant wave height, H_{m0}, of 1.4 m and peak period, T_p, of 5 s. Bed material consisted of sand with a D_{50} of approximately 0.2 mm. During the test substantial dune erosion took place.

Based on the integral wave parameters H_{m0} and T_p and a standard Jonswap spectral shape, time series of wave energy were generated and imposed as boundary condition. Since the flume tests were carried out with first-order wave generation (no imposed super-harmonics and sub-harmonics), the hindcast runs were carried out with the incoming bound long waves set to zero ('first order wave generation'). Active wave reflection compensation was applied in the physical model, which has a result similar to the weakly reflective boundary condition in XBeach, namely to prevent re-reflecting of outgoing waves at the wave paddle (offshore boundary).

A grid resolution of 1 m was applied and the sediment transport settings were set at default values. For the morphodynamic testing the model was run for 0.8 hours of hydrodynamic time with a morphological factor of 10, effectively representing a morphological simulation time of 8 hours.

Test results are given for the root mean square wave height, H_{rms}, and the root mean square orbital velocity, U_{rms}, separated in high-frequency (frequencies above $f_p/2$ corresponding to incident waves) and low-frequency parts (corresponding to infragravity waves). In XBeach model terms, these parameters are defined as follows:

$\mathrm{H}_{rms,HI} = \sqrt{< H^2 >}$

$\mathrm{u}_{rms,HI} = \sqrt{< u_{rms}^2 >}, u_{rms} = \frac{1}{\sqrt{2}} \frac{\pi H}{T_p sinh(kh)}$

$\mathrm{H}_{rms,LO} = \sqrt{8 < (\eta - < \eta >)^2 >}$

$\mathrm{u}_{rms,LO} = \sqrt{< (u^L - < u^L >)^2 >}$

Figure 5.19

In Figure 5.19 the results are shown for first order wave generation (as in the flume tests). The model is clearly capable of capturing both the HF and LF wave heights and orbital velocities. For this test, the agreement is better if incoming bound long waves are omitted from the flow boundary condition (as they were in the laboratory test).

Figure 5.20

In Figure 5.20 the horizontal distribution of sedimentation and erosion after 8 hours is shown, and the evolution in time of the erosion volume and the dune retreat. We see a good agreement for all three parameters. Noteworthy is the episodic behaviour of the dune erosion, both in measurements and model, although the almost exact (deterministic) reproduction of the (stochastic) dune retreat must be a coincidence. An important conclusion for physical model tests is that for dune erosion it does make a difference whether first-order or second-order wave steering is applied.

Figure 5.21

A key element in the modelling is the avalanching algorithm; even though surfbeat waves running up and down the upper beach are fully resolved by the model, without a mechanism to transport sand from the dry dune face to the beach the dune face erosion rate is substantially underestimated. The relatively simple avalanching algorithm described above, whereby an underwater critical slope of 0.3 and a critical slope above water of 1.0 are applied, proves to be quite successful in representing the retreat of the upper beach and dune face. In Figure 5.21 the measured and modelled bed evolution are shown, which looks quite good in the upper region.

Arcilla, A. S., J. A. Roelvink, B. A. O'Connor, A. Reniers, and J. A.Jimenez (1994), *The Delta flume '93 experiment*, in Coastal Dynamics '94, edited by A. S. Arcilla, N. C. Kraus, and S. J. F. Marcel, pp. 488-502, Am. Soc. of Civ. Eng., Reston, Va.

Van Rijn, L.C., D. J. R. Walstra, B. Grasmeijer, J. Sutherland, S. Pan, J. P. Sierra, *The predictability of cross-shore bed evolution of sandy beaches at the time scale of storms and seasons using process-based Profile models*, Coastal Engineering, Volume 47, Issue 3, January 2003, Pages 295-327, ISSN 0378-3839, DOI: 10.1016/S0378-3839(02)00120-5.

5.2.2.2 Bar evolution

Figure 5.22

Figure 5.23

Figure 5.24

Figure 5.25

Figure 5.26

Figure 5.27

5.2.3 H4357: Effect wave period on dune erosion

5.2.3.1 Detailed analysis (T01)

The aim of this test is to make a detailed comparison between simulated physics over an evolving bathymetry and the measurements obtained during the Deltaflume experiment in 2006 (Van Gent et al, 2008). For brevity this comparison is performed only for test T01 (this test corresponds best to the Dutch normative conditions). The simulations is performed on a regular grid with dx = 1 m and input to the model are time series of short wave varying energy (low pass filtered on the wave group time scale) and incoming (bound) long waves. The time series are constructed from pressure and flow measurements at x = 41 m from the wave board. The short wave group velocity (associated with advection of wave action) is based on the Tm-1,0 wave period. Other model settings can be found in Van Thiel de Vries

(2009).

Wave height transformation and wave setup (Figure 5.28) are favourably reproduced with the model. The long wave height is slightly underestimated whereas the wave setup is slightly overestimated. The correlation between measured short wave variance and long wave water surface elevations (Figure 5.29) corresponds reasonably well with the measurements. Towards the shoreline this correlation increases (Abdelrahman and Thornton, 1987; Roelvink and Stive, 1989) meaning the highest short waves travel on top of long waves likely, which likely causes that more short wave energy gets closer to the dune face.

Short wave skewness and asymmetry are reasonably predicted with the extended Rie-necker Fenton model (Figure 5.30, panel 1). However, in the inner surf zone both wave skewness and asymmetry are overestimated. Possible explanations are wave breaking, which limits the steepness and height of waves and the presence of free harmonics in the flume. Both these effects are not included in the wave shape model but indeed are present in the flume test (see Van Thiel de Vries, 2009). From simulated skewness and asymmetry it follows that the total nonlinearity of a short wave is overestimated close to the dune face (Figure 5.30, panel 2). The phase Beta is favourably simulated with the model but is underestimated further offshore.

Figure 5.28

Figure 5.29

Figure 5.30

The simulated test and depth averaged flow velocity shows the same trend as in the measurements and increases towards the shoreline (Figure 5.31). However, in the simulation the cross-shore range with a high offshore mean flow is smaller and extends less far seaward than in the measurements. This is possibly explained by differences in profile development (Figure 5.35) or inaccurate measurements. In addition, another explanation may be found in the incorrect modeling of the roller energy dissipation. Simulations (not shown) with a smaller roller dissipation rate revealed that roller energy in the inner surf increases, leading to higher return flow over a broader cross-shore range.

Long waves contribute to the time and depth averaged flow close to the shoreline. The contribution of long waves to the mean flow is explained by on average larger water depths during the interval associated with shoreward flow velocities in relation to the interval with offshore flow velocities. Considering continuity and a uniform vertical structure of the long

wave flow this means a time and depth averaged offshore directed flow should be present.

Nonlinear waves may cause onshore sediment transport presuming non-uniform sediment stirring over the wave cycle and a positive correlation between sediment suspension and the intra wave flow. In order to include the wave averaged effect of nonlinear waves on the sediment transport a mean flow uA is computed, which is added to the mean (Eulerian) flow Um (see Van Thiel de Vries et al., 2009). The simulated time averaged flow associated with nonlinear waves shows a comparable evolution as in the measurements but is overestimated especially closer to the dune face. Near the shoreline the wave skewness related sediment transport vanishes (Figure 5.30, panel 1) since waves develop towards fully saw tooth shaped bores that have negligible skewness.

The orbital flow velocity (Figure 5.28, panel 2) is favourably predicted by the model. The short wave orbital flow velocity is slightly overestimated whereas the long wave orbital flow is underestimated. The underestimation of the simulated long wave orbital flow corresponds well to the slight underestimation of the observed long wave water surface variance.

Figure 5.31

The simulated test and depth averaged sediment concentration increases towards the shoreline but is underestimated, especially in deeper water where the modeled sediment concentration is smaller (Figure 5.32). In the proximity of the dune face the simulated mean sediment concentration is within a factor two with the measurements. Further offshore the discrepancy between simulations and measurements is larger. The sharp rise in the near dune sediment concentration compares well with the bore averaged near-bed turbulence intensity (Figure 5.33) that also increases towards the shoreline. This increase in turbulence intensity through the inner surf is explained by more intensive wave breaking (turbulence pro-duction at the water surface increases) and by decreasing water depth (generated turbulence at the water surface is more effective in reaching the bed).

The simulated time averaged sediment transport compares well with the measured sediment transport computed from profile changes (Figure 5.34, panel 1). Sediment is eroded from the dune face via avalanching and as a result the sediment transport associated with avalanching is dominant over the dune face and in the swash zone. From the swash zone seaward, the flow based sediment transport becomes more important. At 205 m from the wave board, in

a water depth that varies between 0.1 m and 0.2 m, the flow related sediment transport is dominant.

The simulated flow related sediment transport is separated in sediment transports as-ociated with nonlinear waves (SW), long waves (SL) and the short wave driven under-tow (SR) (Figure 5.34, panel 2):

formula

The offshore sediment transport results from the short wave and roller driven under-tow (SR) combined with the transport associated with the long waves (SL). The transport that follows from the short wave undertow is dominant in the present simu-lation but the long wave related sediment transport cannot be neglected (about 30% at the location of the maximum offshore transport). The wave related sediment transport (SW) is onshore and suppresses the offshore sediment transport with some 30%.

Profile evolution and dune erosion volumes are favourably predicted with the model during test T01 (Figure 5.35 and Figure 5.36, panel 2). Between t = 2.04 and 6.0 hours (in-terval E) the dune erosion rate is slightly underestimated. At the offshore edge of the developing foreshore, the model seems not capable to reproduce the steep transition from the original (unaffected) profile towards the newly developed foreshore. A bar type feature is observed at this transition that is hypothesized to be related to (partly) plunging breakers that generate a water jet, which penetrates in the water column and causes additional sediment stirring when it reaches the bed. Though the effect of wave breaking induced turbulence on sediment suspension is included in the simulation, the applied model only considers spilling breakers, which are expected to be less efficient than plunging breakers in stirring up sand.

Figure 5.32

Figure 5.33

Figure 5.34

Figure 5.35

Figure 5.36

It is concluded that profile evolution and dune erosion during test T01 are favourably simulated. Also simulated wave heights, flows, sediment concentrations and sediment transports compare reasonably well with measurements. However,looking at the results in more detail some discrepancies are found:

1. The long wave height and especially associated long wave orbital flows are un-derestimated.
2. The test and depth averaged flow between x = 170 m and x = 200 m is underestimated. Close to the shoreline no reliable measurements are available to ver-ify the model results.
3. The simulated sediment concentration compares well with measurements close to the dune face. However, for smaller sediment concentrations in deeper water the simulated concentration is underestimated.

4. The offshore sediment transport is mainly driven by the short wave and roller induced undertow (O(70%) at the location of the maximum offshore transport) whereas the offshore directed long wave related sediment transport cancels out with the onshore sediment transport due to nonlinear short waves.

It is remarked that shoreward of the maximum offshore sediment transport, the importance of the long wave related transport increases and eventually becomes dominant in relation to the transport associated with short wave and roller driven under-tow. Considering the mainly long wave associated sediment transport in proximity of the dune face and the importance of long wave run-up for avalanching it is expected that long waves are mainly responsible for the swash zone sediment transport.

Table 5.7

REFERENCES

5.2.3.2 Effect of the wave period (T01, T02, T03)

During test T01, T02 and T03 of the 2006 Deltaflume experiment (Van Gent et al., 2008) the effect of the wave period on dune erosion was examined. It was found that the dune erosion volume increases for a larger wave period, which is caused by a larger flow related sediment transport. In addition, the increase in flow related sediment transport is mainly a result of a higher mean sediment concentration whereas the time and depth averaged flow velocity has the same order of magnitude within the range of wave periods examined.

The aim of this subsection is to examine the processes, which cause the wave period effect in the model and to what extent these processes are in line with the mechanisms observed in the measurements. To this end test T01, T02 and T03 of the Delta-flume experiment are simulated. The simulations are performed on a regular grid with dx = 1 m and input to the model are time series of short wave varying energy (low pass filtered on the wave group time scale) and incoming (bound) long waves. The time series are constructed from pressure and flow measurements at x = 41 m from the wave board. The short wave group velocity (associated with advection of wave action) is based on the Tm-1,0 wave period. Settings for the wave energy dissipation model are found in Table 1 and other setting are defaults as listed in in Appendix X.

formula

In Figure 1 simulated profile evolution during the tests compares well with the measured profile evolution. However, the bar type feature at the offshore edge of the developing foreshore is not reproduced in the simulations. Comparing measured and simulated dune erosion volumes in Figure 2 it is seen that for test T03 the erosion volume after 1 hour and 2.04

hours of waves is underestimated whereas for test T01 and T02 simulated erosion volumes are reasonably well predicted over all test inter-vals.

Figure 1 Simulated profile evolution (dashed lines) for test T01 (upper panel), test T02 (middle panel) and test T03 (lower panel) compared with measured profile evolution (solid lines) after t = 0.0, 0.1, 0.3, 1.0, 2.04 and 6.0 hours.

Figure 2 Simulated dune erosion volume above still water level (dashed lines) for test T01 (open squares), T02 (open triangles) and T03 (open circles) compared with measured dune erosion volume (solid lines) for test T01 (closed squares), T02 (closed triangles) and T03 (closed circles) as function of time.

Simulated time and depth averaged flows are compared in Figure 3, which shows that the mean flow slightly increases with a larger wave period (6% between x = 170 m and x = 205 m). This tends to be a slightly different trend than observed in the measurements that show a 3% increase in the same cross-shore area. It is remarked though that any firm conclusions cannot be made since the measured time and depth averaged flow velocities are based on limited sensors over depth (and for that reason it was concluded that the mean flows for test T01 and T03 are compa-rable).

The increase in the simulated offshore directed mean flow is caused by an increase of the short wave related mass flux whereas the roller related mass flux is only slightly different. The maximum long wave related mean flow is larger during test T01 than during test T03.

Figure 3 Simulated test and depth averaged flow associated with short waves (dashed-dotted line), rollers (dotted line) and long waves (dashed line) for test T01 (left panel) and test T03 (right panel). The simulated total test and depth averaged flow (solid line) is com-pared with measurements (squares).

Simulated sediment concentrations are compared with measurements in Figure 4 and show an O(60%) increase in the mean sediment concentration for a larger wave period between x = 170 m and x = 205 m. This increase is comparable as observed in the measurements (O(60%) for the test and depth averaged sediment concentration). The simulated mean sediment concentration is underestimated with O(40%) com-pared to the measurements between x = 170 m and x = 205 m for both model simulations.

Figure 4 Simulated mean sediment concentration (solid line) compared with test and depth averaged sediment concentrations obtained from the suction tubes (squares) for test T01 (left panel) and test T03 (right panel).

It is concluded that the effect of the wave period on dune erosion and dune face retreat is favourably predicted with the XBeach model. The simulated increase in dune erosion with a larger wave period is mainly caused by an increase of the mean sediment concentration of O(60%), which is comparable to the measurements. The near dune return flow slightly increases with approximately 6% for a larger wave period. However, the accuracy of measured time and depth averaged flows is insufficient to verify this increase.

The following results are obtained during the last test run:

Figure 5.37

Figure 5.38

Figure 5.39

Figure 5.40

Figure 5.41

Figure 5.42

5.2.3.3 Effect of spectral shape (DP01, DP02)

Test DP01 and DP02 were conducted with a double-peaked wave spectrum to investigate what (spectral) wave period is best qualified to describe dune erosion (Van Gent et al., 2008). In this document the tests are discussed to obtain further insight in the capability of the model to simulate dune erosion for various wave spectra. The simulations are performed on a regular grid with dx = 1 m and input to the model are time series of short wave varying energy (low pass filtered on the wave group time scale) and incoming (bound) long waves. The time series are constructed from pressure and flow measurements at x = 41 m from the wave board. The short wave group velocity (associated with advection of wave action) is based on the Tm-1,0 wave period. Settings for the wave energy dissipation model are found in Table 1 and other setting are defaults as listed in in Appendix X.

Simulated and measured profile evolution and dune erosion volumes for test DP01 and DP02 are compared in Figure 1 and Figure 2 respectively. For test DP01 the profile evolution is accurately reproduced and results for test DP02 are reasonable even though the erosion rate during the last interval is overestimated.

Figure 1 Simulated profile evolution (dashed lines) compared with the measured profile evolution (solid lines) for test DP01 (upper panel) and test DP02 (lower panel) after t = 0.0, 0.1, 0.3, 1.0, 2.04 and 6.0 hours for test DP01 and 1.0, 2.04 and 6.0 hours for test DP02.

Figure 2 Simulated dune erosion volume above still water level (dashed line with open squares) compared with measured dune erosion volume (solid lines with closed squares) as function of time for test DP01 (left panel) and test DP02 (right panel).

The imposed double-peaked wave spectra affect the time scale and amplitude of the simulated wave groups. Consequently, the interaction of simulated long waves with the short wave groups is different and hydrodynamics in front of the dune face are expected to have other characteristics. In Figure 3 the simulated wave transforma-tion, flows and sediment concentrations are favourably compared with measurements obtained during test DP01. It seems the model is capable to take into account the ef-fect of various wave spectra on near dune hydrodynamics and sediment transports.

Figure 3 Upper left panel: Simulated wave setup (dotted line) and transformation of the total (solid line), short (dashed line) and long (dashed-dotted line) wave height compared with measurements of the setup (circles) and the total (squares), short (upward triangles) and long (downward triangles) wave height. Upper right panel: Transformation of the simu-lated total (solid line), short (dashed line) and long (dashed-dotted line) wave orbital flow ve-locity compared with the measured total (squares), short (upward triangles) and long (down-ward triangles) wave orbital flow velocity as function of the cross-shore position. Lower left panel: Simulated test and depth averaged flow Um due to short and long waves (solid line) and long waves only (dashed line) as function of the cross-shore position. The dotted line corresponds to the wave averaged sediment advection velocity uA due to nonlinear waves. Markers correspond to measured undertow flow velocities due to short and long waves (downward triangles) and the measuredXVI mean flow due to nonlinear waves (upward triangles). Lower right panel: Simulated mean sediment concentration (solid line) compared with the measured time and depth averaged sediment concentrations (squares) as function of the cross-shore distance.

It is concluded that the effect of the wave spectral shape on dune erosion and dune face retreat is favourably predicted with the model. The time averaged simulated wave transforma-tion, flow and sediment concentration compare well with the mobile frame measurements obtained during test DP01.

In Van Gent et al. (2008) the spectral mean wave period Tm-1,0 is argued to be more qualified to describe dune erosion than the peak wave period Tp. The simulations presented in this subsection are performed with the Tm-1,0 wave period and show satisfying results suggesting the spectral mean wave period proposed by Van Gent et al. is indeed a good measure to describe dune erosion. It is remarked though that any firm conclusion would require extra simulations in which the peak wave period Tp is applied instead of the Tm-1,0 wave period. In addition this would demand for a new model optimization and most likely different settings for the wave dissipation model.

The following results are obtained during the last test run:

Figure 5.43

Figure 5.44

Figure 5.45

Figure 5.46

Figure 5.47

Figure 5.48

5.2.3.4 Double dune system (T04)

Test T04 of the Deltaflume experiment 2006 (Van Gent et al., 2006) is carried out with an initial profile that contains a small dune in front of a larger volume dune that collapses after approximately one hour of waves (interval C and D). After breaching of the small dune, the foreshore is already very efficient in reducing wave impacts on the dune face resulting in small erosion rates over the remaining test intervals. In this test it is examined to what extent the dune breach can be reproduced with the XBeach model and whether the (substantially smaller) erosion rate at the end of a storm is correctly predicted. The simulations is performed on a regular grid with dx = 1 m and input to the model are time series of short wave varying energy (low pass filtered on the wave group time scale) and incoming (bound) long waves. The time series are constructed from pressure and flow measurements at x = 41 m from the

wave board. The short wave group velocity (associated with advection of wave action) is based on the Tm-1,0 wave period. Settings for the wave energy dissipation model are found in Table 1 and other setting are defaults as listed in in Appendix X.

formula

Figure 1 Simulated profile evolution (dashed lines) compared with measured profile evolution (solid lines) for test T04 after t = 0.0, 0.1, 0.3, 1.0, 2.04 and 6.0 hours.

Figure 2 Simulated dune erosion volume above still water level (dashed line with open squares) compared with measured dune erosion volume (solid lines with closed squares) as function of time for test T04.

Simulated profile evolution and dune erosion volumes are shown in Figure 1 and Figure 2 respectively. For the first three intervals (the small dune breaches in interval 3) the dune erosion rate is slightly overestimated but the profile evolution compares favourably with the measured profiles. Considering the last two intervals, erosion rates and dune face retreat are too large.

Breaching of a small dune in front of a larger volume dune causes that suddenly the foreshore is significantly closer to equilibrium with the storm surge conditions. As a result near shore hydrodynamics, near shore sediment transports and wave impacts on the dune face are less severe. It is concluded that the feedback between profile evolution and near dune processes is not sufficiently well included in the model at the end of test T04, which is representative for conditions at the end of a storm. More insight in the model performance at the end of a storm could possibly be obtained by comparing the evolution of simulated driving processes (undertow, sediment concentrations and avalanching) with measurements.

The following results are obtained during the last test run:

Figure 5.49

Figure 5.50

Figure 5.51

5.3 Small scale tests

5.3.1 H4265: Effect wave period on dune erosion

5.3.2 1202124-007: Dune erosion and overwash at wide beaches

5.4 Longshore effects

5.4.1 H5109: Interaction between dunes and dikes

Chapter 6

Morphological field tests

6.1 1953 storm surge

In order to test the model performance in prototype conditions, this test studies the impact of the 1953 storm surge on the Dutch coast at Delfland. The initial profile for the simulation is obtained from test T4 of the M1263-III experiment conducted in the Deltaflume (Vellinga, 1984) and is scaled-up to prototype. The profile is representative for the coast at Delfland. The applied grid is uniform with dx = 4.56 m and the applied hydrodynamic conditions vary over the storm (see Figure 6.1). Simulation settings are default except for the maximum erosion rate dzmax, which is scaled-up to 0.17 m3/ms applying the scale relation for the erosion volume (Vellinga, 1988).

Figure 6.1

Simulated profile evolution is shown in Figure 6.2. The erosion volume above maximum storm surge level is about 100 m3/m. This is in reasonable agreement with the measured erosion volumes (above storm surge level) after the 1953 storm surge which had a mean value of 90 m3/m and a standard deviation of 26 m3/m. At the end of the storm surge the dune foot is located approximately 1 m above the maximum storm surge level.

Evolution of the simulated dune erosion volume is shown in Figure 6.3. It is concluded the simulated erosion volumes are in reasonable agreement with the observed erosion volumes at delfland after the 1953 storm surge. In addition the evolution of the simulated dune erosion volume reveals that most dune erosion occurs in a relatively short time interval between t = 10 hours and t = 15 hours when the mean water level is increasing towards the maximum storm surge level. After the peak of the storm surge the erosion rates are relatively small. At the end of the storm surge the dune foot in the simulations is located approximately 1 m above the maximum storm surge level.

Figure 6.2

Figure 6.3

6.2 1976 storm surge

6.3 Asseteague Island

Besides well-controlled laboratory cases, the model is also applied to the field. The first example concerns the morphodynamic response of sandy dunes to extreme storm impacts at Assateague Island, Maryland, USA, which was analyzed before by Jimenez et al (2006). Two consecutive northeasters attacked the barrier island during late January and early February, 1998. The bathymetry was measured using LIDAR in September 1997 and again February 9th and 10th, 1998 after the two storms had subsided.

Three types of dunes were identified by Jimenez et al (2006), shown in Figure 6.4. Profile A (upper left panel) is initially characterized by a steep faced dune, where the maximum run-up exceeded the dune crest height and the mildly sloped back of the dune. The morphological response is characterised by profile lowering, decrease of the beach face slope and landward barrier displacement, while retaining barrier width.

Profile type B is a double-peaked dune profile and has two different shapes. Profile B1 (upper right panel) is initially characterized by a primary and secondary dune, both of which are lower than the maximum run-up height and which are separated by a valley. Profile B2 (bottom left panel) initially has two peaks of which the seaward one is lower. The backside of the barrier of either type is therefore either characterized by a secondary dune line (profile B1) or a taller crest of the dune (profile B2) which prevents the eroded sand from being transported to the backside of the dune. The main morphological response for these profile types is a decrease of the beach face slope, outer shoreline retreat and narrowing of the barrier.

The height of the dune crest of profile C (lower right panel) exceeds the maximum run-up height and so little overwash is observed. The morphological response of this type of profile is crest lowering due to slumping, decrease of the beach face slope and retreat of the outer shoreline. The width of the barrier is seen to decrease.

The storm impact of the two North Easters on Assateague Island were modelled with XBeach for the four profiles described by Jimenez et al. (2006). The profiles were extended with a shallow foreshore and a 1:100 slope in seaward direction till a water depth of 9 m below NAVD88. As XBeach has not been shown to accurately simulate morphological change during very long storm durations, the simulations were run for a total of 20 hours. The measured wave and surge conditions were parameterized for each storm by a constant surge level and a constant wave spectrum (Pierson-Moskowitz) (see Table 6.1). This approach assumes that two 72 hour storms with varying surge and wave conditions can be approximated by two 10 hour simulations with constant maximum surge and wave conditions following a similar approach as Vellinga (1986). This approach also facilitates further sensitivity studies into the effect of varying hydraulic forcing conditions. The calculation grid size varies from 18 m at the offshore boundary to 2 m on the islands. A morphological acceleration factor of 5 is applied. The final simulated bed profiles are shown in Figure 6.4.

Table 6.1: Hydrodynamic boundary conditions XBeach simulations

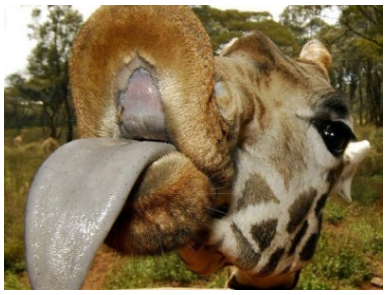

Figure 6.4: Pre-storm profiles (black dotted line), measured post-storm profiles (black solid line) and modelled post-storm profiles (red solid line). Upper left panel: profile A. Upper right panel: profile B1. Lower left panel: profile B2. Lower right panel: profile C. The seaward side is on the left in all panels. Note that the measured post-storm profiles contain only the sea surface and emerged topography and no submerged topography.

The profile changes calculated by XBeach are largely consistent with the description of dune evolution given by Jimenez et al (2006). Jimenez et al observed that profile A became flatter, with large quantities of eroded sediment deposited on the back side of the barrier island, due to the consistent wave over-topping. The model replicates this behaviour, except that the island is lowered more than in the measurements and that the seaward face of the island does not roll back as it does in the measurements.

The observed response of profile B1 was dune face retreat, overwash deposition in the dune valley between the primary and secondary dunes and narrowing of the island, Jimenez et al (2006) also noted decrease of the beach face slope. It can be seen in Figure 6.4 that the morphological development of the island is well represented by the model. The simulated dune crest retreat corresponds closely to the measured retreat. Overwash takes place in the model and sediment is deposited in the valley between the primary and secondary dunes, although the magnitude of deposition is less than in the measurements.

The XBeach model of profile B2 shows a slope reduction on the seaward side and lowering of the seaward dune. The second dune crest retains its crest level as described in the work of Jimenez et al (2006). The beach slope decrease in the XBeach model is in line with the

description given by Jimenez et al (2006), but differs from their measured profile. It is unclear why the measured profile shows almost no erosion of the beach face.

Jimenez et al. (2006) observed, in general, profile C to lower in height, the seaward dune slope to become smaller, and seaside retreat of the shoreline resulting in barrier narrowing. The XBeach model shows retreat of the upper dune face and a reduction of the seaward dune slope. The model over predicts the sedimentation at the base of the dune and under predicts the crest lowering.

Jimenez, J.A., Sallenger, A.H. and Fauver, L., 2006. *Sediment transport and barrier island changes during massive overwash events*, ICCE 2006, San Diego.

Vellinga, P., 1986. *Beach and dune erosion during storm surges.* PhD Thesis, Delft University of Technology.

6.4 Zwin

Having examined two-dimensional hydrodynamics, we move to 2D morphodynamics. The next test carried out is that on the Zwin breach growth experiment, as reported by Visser (1998). In the mouth of the Zwin, a tidal inlet located at the border between the Netherlands and Belgium, an artificial dam was constructed with a crest height of 3.3 m +N.A.P. (Dutch datum, approx. MSL), crest width 8 m, inner slope 1:3 outer slope 1:1.6 and length 250 m. An initial depression of 0.8 m was made in the middle of the dam having a width of 1 m and a side slope of 1:1.6 to ensure that the breach initiated at this location. The level of the surrounding sea bed was about 0.7 m + N.A.P. The mean tidal prism of the Zwin is about 350,000 m3. The polder area A_p as a function of the water level behind the dam is given by:

$A_p = (170.000m)z_s - 100.000m^2, 0.6m < zs < 2.3m + NAP$

$A_p = (2.100.000m)z_s - 4.540.000m^2, zs > 2.3m + NAP$

At t = 0, about 10 minutes prior to high water, the water level at the seaside was NAP + 2.72 m. At t = 10 minutes a water level of 2.75 m + N.A.P. was reached. For the remainder of the test, which had a total duration of 1 hour, the water level marginally decreased. After 1 the breach growth became nil, as the water level of the polder area behind the breached equaled the sea level. The wave height near the dam was negligible during the experiment. The wind speed was about 2 m/s.

Until t = 6.5 minutes the breach depth grew whereas the breach width remained constant. At t = 6.5 minutes the original dike structure had nearly completely disappeared over the initial depression width of 1 m. Near t = 6.5 minutes the onset of lateral breach growth was observed. The scour hole developed further down to a depth of 1.6 m -N.A.P. (4.9 m below the original dam crest level). The rate of lateral breach growth was about 2 cm/s. After approximately 40 minutes the process slowed down considerably and after approximately one hour the water levels at both sides were equal.

A schematized representation of the Zwin test was created in XBeach, with at the sea side a uniform bed level at 0.7 m +NAP, and inside the basin a prismatic profile with the deepest point at 0.7 m + NAP and sloping sides, such that the polder area as a function of the water level was in accordance with the equations above. The grid is non-equidistant with grid sizes gradually varying from 0.5 m near the breach to approx. 50 m far away from it. The median grain diameter D50 of the bed material was set to 0.3 mm in accordance with the prototype test conditions for the artificial dam. The applied critical slopes for avalanching are the same

as in other tests and standard settings were applied for the transport formulations. Waves were negligible in the test and were set to zero. The model was run with a CFL of 0.5 and remained smooth and stable despite the steep slopes and supercritical flows.

In Figure 6.5 a sequence of 3D images is shown depicting the various stages in the breaching process: the initial overflowing, the cutting back of the breach, the deepening and finally the widening of the breach. Qualitatively and quantitatively the results are in agreement with the experiment by Visser (1998), although details may be different due to the schematized initial bathymetry.

Figure 6.5

In Figure 6.6 a comparison is given between measured and simulated water levels, flow velocities and development of the breach width in time. Observation point MS2 is 30 m upstream of the centre point of the breach and MS4 is 30 m downstream of it. In MS4 there was some ambiguity in the measured initial water level, which explains the initial discrepancy between measurements and simulations. The slight reduction in water level at the end of the measurement in MS2 is due to a rather narrow channel that was present in reality but not in the model, which causes higher velocities than in our model and a reduction of the mean water surface. In spite of these differences, the overall agreement for the development of the velocity in MS4 and for the breach widening is quite satisfactory. Measured and simulated flow velocities compare reasonably well in MS4.

Figure 6.6

Visser, P.J. 1998. *Breach growth in sand dikes.* Ph.D.-thesis Delft University of Technology, the Netherlands.

6.5 MICORE field experiments

6.5.1 Lido di Dante, Italy

The study site is the Lido di Dante-Lido di Classe area, an 8 km stretch of sandy beaches along the Emilia-Romagna coastline in northern Italy on the Adriatic Sea. The site is a mixture of urbanised (approximately 40% of the total area) and relatively pristine (approximately 60%) coastal environments. The seaside towns of Lido di Dante and Lido di Classe are located at the site's northern and southern boundaries respectively. In these regions the beaches are protected by offshore breakwaters and groins and backed by moderate coastal development in the form of beach huts, holiday accommodation and paved roads. Between these two towns is a natural park consisting of natural vegetated dunes and no coastal protection. Three river mouths are located at the site: one at Lido di Dante (Fiumi Uniti); one at Lido di Classe (Fiume Savio); and one in the centre of the natural park (Torrente Bevano).

The submerged beach is generally composed of fine sand, while the beachface is made up of fine to medium sands (D50 = 0.03 mm). The intertidal beach slope varies significantly along the 8 km's of coastline, from mild (2.5%) to steep (14%). Steep values are representative of areas adjacent to coastal defence structures (i.e. groins) while the area inside the natural park is characterised by lower gradients. The mean submerged beach slope is 3%. According to the morphodynamic classification of Wright and Short (1984), the beaches are considered as having intermediate beach states. Low tide terraces are often observed both in the protected and natural areas. Submerged longshore bars meanwhile are only present in the areas outside of the offshore structures.

The wave climate of this region is generally small, with 91% of significant wave heights below 1.25 m. The prevalent wave direction is from the east, while the most intense storms are from the ENE (known as the "Bora wind"). The Bora wind is a strong, cold, gusty wind that blows

intermittently but mainly during the winter months. It not only has a strong influence on the wave climate of this region, but of the general circulation patterns of the entire Adriatic Sea. South-easterly waves meanwhile are much less significant, since SE winds are sheltered to some degree by the Conero Headland approximately 120 km south of the site.

In regards to water level variations, the area is microtidal with a mean neap tidal range of 30-40 cm and a mean spring tidal range of 80-90 cm. The tidal signal has both diurnal and semidiurnal components. Tidal anomalies of up to double the maximum tidal elevation can occur as a result of surge. This is particularly the case during SE wind conditions, where, considering the SE-NE orientation of the Adriatic Sea, there is the greatest fetch for wind-driven surge.

Within the 2008-2010 MICORE monitoring period, three storms were selected for calibration of the off-the-shelf and XBeach models. Each storm has distinct properties that encompass the range of storm conditions typical for the Emilia-Romagna region. Here the modelling is restricted to profile MN15 for the 1-3 December 2008 storm.

At this stage XBeach substantially overestimates erosion (see Figure 6.7). Whereas measurements indicate only moderate frontal dune erosion, (excluding MS17 for the 1-3 December 2008 storm) the dune is overtopped and completely destroyed in the simulations. The results even indicate erosion into the artificially-generated 3m dune placed at the back of the profile.

Because of the large disparity between the XBeach model and measurements for Italy, quantitative analysis of the results has not been conducted at this stage.

Figure 6.7

6.5.2 Praia de Faro, Portugal

The study area is Ancao Peninsula constituting the westernmost barrier of the Ria Formosa barrier island system. It is a NW-SE oriented sandy barrier that is attached to mainland by its western terminus.

The area is mesotidal, with an average tidal range of about 2 m that can reach up to 3.5 m during spring tides. Analysis of two years of records from a tidal gauge on the Algarve Coast showed a maximum observed storm surge level of +0.75 m (Gama et al., 1994). The return

period of a sea level 2.23 m above Mean Sea Level (MSL) is 10 years (Gama et al., 1994).

The offshore wave climate is dominated by west-southwest waves (71% of occurrences). SE waves that consist of short period waves generated by regional winds (locally called 'Levante') are also frequent (about 23%). Wave energy is moderate with an average annual significant offshore wave height of 1.0 m and average peak period of 8.2 s (Costa et al., 2001).

Storm events in the region are considered when the significant offshore wave height exceeds 3 m (Pessanha and Pires, 1981) and typically correspond to less than 1% of the offshore wave climate (Costa et al., 2001). A 5.0 m significant wave height for a SE storm has a return period of 50 years, whilst a 5.7 m SW storm is expected every 5 years (Pires, 1998). Due to it's northwest-southeast orientation it is directly exposed to west-southwesterly waves, and is relatively protected from SE waves.

Several storm events have been recorded during the MICORE campaign among which the two most important are discussed in the MICORE report. Here a group of several individual WSW storms is simulated that took place at Faro beach from 18/12/2009 until 5/1/2010. The significant wave height reached 4 m and the peak period up to 20 sec, while given the long duration intense wave conditions coincided with both spring and neap tides. The event had a significant impact on the coast, as overtopping and dune erosion occurred at several sections.

The obtained simulation results with XBeach were in general not satisfactory as they result in negative BSS values. Apart from the unrealistic berm erosion, another significant difference between the measured and simulated profiles is that upper profile change in Faro beach appeared to decelerate during the storm period (see Figure 6.8), a behavior which the model did not appear to follow. After the morphological change of the first storms, the beach appeared to reach a new 'equilibrium state', which was affected only when storm conditions coincided with exceptionally high tidal levels. On the other hand, current XBeach modelling efforts resulted in erosion even in these equilibrium conditions.

Another deviation from the field observations, apart from the increased berm erosion and scarping, is a narrower profile section with morphological change, compared to the one shown by the data.

Figure 6.8

6.5.3 Cadiz Urban Beach, Spain

The field site is located around Cadiz town, in south-western Spain, facing the Atlantic Ocean. It is constituted by two different beaches extending along 10 km, providing the opportunity for studying the effects of storms on different types of coastal environments.

The study area is a mesotidal coast with a mean tidal range of 3.2 m and 1.1 m during springs and neaps tides, respectively. Dominant winds blow from ESE (19.6% of annual occurrence) and WNW (12.8%), which together with coastline orientation makes sea and swell waves approach generally from the third and fourth quadrants. According to this, prevailing longshore drift is directed south-eastwards. Significant wave height is usually lower than 1 m, with waves over 4 m high being uncommon and occurring only during the most important storms, which usually take place between November and March and approach from the third quadrant. In fact, waves greater than 1.5 m are considered storm waves, so the area can be classified as a low-energy one.

The storm event that was selected is a moderate storm event with a return period of about 1 year. The maximum significant wave (Hs) height during the peak of the event was 3.7m with a spectral period (Tp) of 8.7sec. The total duration of the storm was 46 hours (light grey shaded area). The tidal conditions over that period were from springs to neaps with an average tidal range of 2.27m.

Both the Xbeach model and the off-the-shelf model Petra were used to predict the morphological changes of the storm described above. Despite the fact that applied models simulate different physical processes, both produce a relative good final profile (Figure 6.9). Nevertheless some discrepancies with the measured profile are present. XBEACH better predicts the near berm erosion and beach slope and PETRA performs better in the intermediate and low intertidal area.

Figure 6.9

6.5.4 Mariakerke and Ostend Beach, Belgium

The Ostend beach (adjacent to Mariakerke), located almost in the middle of the Belgian coast, is a dissipative beach, characterised by a low beach gradient, a surf zone with the presence of

numerous spilling lines of breakers and by fine to medium sandy sediments (D50=0.214 mm). The study area is densely populated with apartment buildings on the dyke and a promenade protected by a seawall without naturally-developed dunes. The coastal defence is designed for to give protection for a T100 storm event (return period of 100 years).

The Belgian coast has a bi-diurnal tide with a small asymmetry and an average tidal range of 4m. The tidal wave moves along the coast from west to east. The tidal range decreases in the same direction by +/- 0.5 m. Spring tides occur twice a month when the tidal variation has reached its maximum (+/- 5 m), while for neap tides occur the tidal range reaches its minimum, i.e. +/- 3 m. The tidal curve has an asymmetric shape because the low tide lasts half an hour longer than the high tide. Meteorological circumstances can significantly influence the curve as well. Long-lasting intense winds may influence the water level, resulting in extremely low or high water levels. This important tidal range is linked to quite significant tidal currents, which exceeds generally 1.5 knots in the near shore areas. Because of the shallow seas and the short fetch, waves are typically short crested at the Belgian coast.

The wave climate along the coast is mainly determined by meteorological circumstances, predominantly westerly winds, and by the shallow depth of the North Sea. Under normal circumstances the wave along the coast is lower than 1 meter. During (heavy) storms wave heights of over 5 meters can occur. The wave period is 3 to 4 seconds under calm weather conditions, but during storms it can reach 10 to 15 seconds (IMDC, 2005).

Between 08/11/2007 0000Z and 1800Z an active depression moves from just southeast of Iceland towards Norway and settles afterwards in south Scandinavia. On the back of this depression, strong northerly wind fields develop and spread over the Norwegian Sea and the North Sea. This situation causes high water levels and waves along the North Sea Coasts (Versluys, 2007).

Currently, beach and dune erosion at the Belgian coast is estimated with Durosta. For the storm of November 2007, calculations have been performed with Durosta for Ostend beach and compared with the measurements. Durosta has been run with default settings. Several profiles (1D) have been modelled on a grid that varies from 6m offshore to 1m near the seawall. The seawall has been included as a non-erodible element.

To compare the performance of XBeach with Durosta, the same 1D-profiles haven been modelled for Ostend beach. The grid in XBeach has been chosen identical to that of Durosta and varies from 6m offshore to 1m near the seawall. The performance of XBeach will be compared with Durosta. Since Durosta is a 1D model, also XBeach has been applied in 1D mode.

In Figure 6.10 the model results from XBeach and Durosta are compared with the measurements for the November 2007 storm at Ostend beach. Additionally the Brier Skill Score has been determined between the dyke and -500m.

Both XBeach and Durosta give a more uniform beach profile than is observed in the measurements. Small bars in the profile are hardly predicted with both models. For the presented results XBeach obtains a better score than Durosta.

Comparing both models it is concluded that XBeach delivers (also for most other cases presented in the WP4 report) a slightly better result than Durosta. Especially the prediction of the beach erosion front seems a bit more accurate in XBeach.

Figure 6.10

6.5.5 Sefton Coast, England

6.5.6 Dziwnow Spit, Poland

The Polish study site is the 14 km long Dziwnow Spit of barrier type built of Holocene deposits (mainly sands) with dunes 3.5 to 10 meters high. Behind the spit there are relatively wide lowlands of glacial or glaciofluvial origin, in most cases filled with peat. Their surface is 1 to 3 m above sea level. In the lowlands alos the Kaminski Lagoon is found with a rather small depth (maximum 2-3 m). At the middle of the spit there is a connection between the lagoon and sea (Dziwna). The mean beach width calculated for the pilot area is 33 m.

The average tide range in the Baltic is very small and is less then 10 cm. This is due to the small area of the Baltic, its geographical situation and the presence of the Danish Straits, which prevent propagation of North Sea tides into the Baltic. Thus, surface waves (wind waves and swell) are the most important factor of the Baltic coastal zone hydrodynamics. The wave climate in Poland is highly diversified because of the wealth of fetches and wind speeds occurring throughout the year.

Since 1 June 2008, (from the beginning of observations taken within MICORE project) 1 extreme storm (12.10.2009) was noticed which caused significant morphological changes at the shore. The storm return period was about 4 years and was simulated with the XBeach model.

The storm occurred on 12.10.2009 and lasted for almost 4 days (93hours). The highest sea level observed on tide gauge located in the Dziwna (Dziwnow Port Authority area) was 0,76 m. above mean sea level. The maximum significant wave height (Hs) reached 3.2 m and teh maximum peak period (Tp) was 11.17 sec.

The XBeach model was run for profile 386 in 1D mode. The profile was interpolated to a cross-shore varying grid with a minimum cell size of 3 m. Offshore wave data timeseries from the WAM model were inputted to XBeach using a Jonswap spectrum and setting instat=41. Wave direction values were changed to 270 degrees, which means that incoming waves are shore normal. Surge input data were taken as the hourly mean sea level.

It is visible from the simulation (see Figure 6.11), that at this stage the amount of dune erosion is avoerestimated by XBeach according to post-storm data.

Figure 6.11

6.5.7 Kamchia Shkorpilovtsi Beach, Bulgaria

The study area, called Kamchia-Shkorpilovtsi, is situated in the western Black Sea, and spreads from cape Paletsa to cape Cherni Nos (Figure 9.1), located 25 and 40 km to the south of Varna city, respectively. It comprises the longest and the largest sandy beach along the Bulgarian Black Sea coast, with well-developed dunes and the two rivers' mouths, these of the Kamchia River and the Fundakliiska River. In the middle of the site, near the mouth of the Fundakliiska River a scientific pier is built perpendicularly to the shoreline, reaching 4.5 m water depth. The beach is formed as a result of accumulation of erosive and fluvial sediments. The main morphological feature of the study area is its rectilinear shoreline with almost parallel isobaths. The bottom slope is covered with sands of different size. In its upper part down to 2.5 m depth, over 95% of bottom sediments consist of coarse and medium sand fractions. As the depth grows, the content of these fractions decreases and at 8-10 m over 90% of the sediment grain size is less than 0.25 mm.

The beach is open to waves of the eastern half. In the case of severe storms the wind speed magnitude can reach 35-40 m/s and 9 m height of maximum significance wave at depths of about 1000 m. The large seasonal variability is one of the most marked features of the wave climate. The winter storms are much more frequent than the summer ones. In the western Black Sea the most frequent are the winds from northeast and east, which trigger the most severe storms.

In the beginning of March a short but very intense storm occurred in the western Black sea. This event was distinguished with all features of the severe storms known from the historical overview well defined phases growth took place on 08.03, peak 09.03 and decay 09.03 - 10.03. Wind and wave direction were quite stable turning from ESE to ENE. Maximum SWH reached almost 4.20 m.

Model results for this storm are shown in Figure 6.12. Both models predict washing out of the upper part of the profile, but XBeach overestimates it significantly. Both models predict

re-deposition of eroded material downward the profile, while in reality such accretion was not observed. Both models predict washing out of the permanent bar, and both of them underestimate the erosion rate.

Figure 6.12

Chapter 7

Comparisons with other models

7.1 Laboratory measurements

7.2 Field applications

7.2.1 Erosion volumes JARKUS

7.2.2 Curved coastlines

Chapter 8

Specific functionalities

8.1 Stationary wave solver

8.2 River outflow

The river outflow case is meant to test the models for the combined effects of a river outflow and a steady wave-driven longshore current on the sediment transport and the morphological evolution. Though purely hypothetical, this case contains many salient features of real-life applications, such as longshore currents through open side-boundaries and exchange of water and sand through a gap in a closed boundary. Thus, the formulation of open boundary conditions is also tested here.

The initial topography consists of a plane beach (slope 1: 50), which is interrupted by a 75 m wide river mouth with a water outflow of 150 m3/s. The bottom contours are straight and parallel to the shoreline, except for a shallow submerged channel in line with the river.

The computational grid is rectangular, with 56 nodes in the x-direction (cross-shore) and 111 nodes in the y-direction (longshore), with a uniform grid spacing of 15 m. The waves are irregular and long-crested, with a root-mean-square height of 2m at a water depth of 13.5 m. The direction of wave incidence is 30 degrees with respect to the shore-normal. The peak wave period is 8 s. The bed material is uniform sand of 250 am, with a settling velocity of 0.031 m/s.

In this figure the bathymetry is shown after approx. 4 days; arrows indicate the sediment transport vectors. plotted for every cross-shore cell and every third longshore cell. When functioning correctly, we see a channel that has turned towards the north and striasght contour lines downstream of the channel.

Figure 8.1

8.3 Drifters

This test combines three specific functionalities of XBeach: curvilinear grids, discharges and drifters. The model is basicly an odd-shaped bathtub with a single discharge location at the left boundary. The bathtub is filled by the discharged water, indicated by the increasing water levels (colored background). The bathtub is approximately 70m x 70m. Considering that, he discharge of $50^3/s$ is rather large. Every 10 seconds, two drifters are released just before the discharge opening. One of the two drifters is released at the upper boundary of the opening, the other at the lower boundary. The entire path a single drifter has followed at a certain moment in time is plotted. Two large eddies driven by the large discharge are revealed by these paths.

Figure 8.2: Drifter paths after 50s

Figure 8.3: Drifter paths after 150s

Figure 8.4: Drifter paths after 450s

8.4 Multiple sediment fractions

The purpose of this simulation is to ensure the multiple sediment fractions model in XBeach performs as expected. In this test, the Deltaflume 2006 T01 test is recreated with two types of sand with different colours, red and blue. The sand is initially placed in a zebra-stripe pattern in the profile. The properties of both types of sand such as the grain size and mobility are the same as the sand used in the Deltaflume experiment. For the test to be successful, the following conditions should be met:

- The simulated final profile should be the same as the final profile in the original Deltaflume 2006 T01 test.

- The two sediment types should mix and form layers over each other.

The figures Figure 8.5 and Figure 8.6 show the initial and final distribution of red and blue sediment in the profile near the dune face. The red and blue lines in the same figure show the sediment concentration of each sediment type in the water column. If the simulation is successful, the red and blue sediment will be well mixed on the foreshore and fresh blue sediment will be deposited over the red sediment at the dune foot as the dune face retreats. The concentration of blue sediment in the water column should be higher than the concentration of red sediment in the water in areas where only blue sediment is available in the top layer of the bed.

The red lines in Figure 8.7 show the predicted dune face retreat and bed level change in the XBeach multiple-sediment model. The black lines in the same figure are the corresponding measured profiles. If the simulation has been successful, the red and black lines will align reasonably well. The results of this simulation should be compared to the Deltaflume 2006 T01 test described earlier in this report.

Figure 8.5

Figure 8.6

Figure 8.7

8.5 Ground water module

8.6 Curvilinear

8.7 MPI vs. serial

8.8 Output